

# Frequency-matching quantum key distribution

Hao-Tao Zhu,<sup>1,2,3,4</sup> Yizhi Huang,<sup>5</sup> Abdullah Rasmita,<sup>1,2,3,4</sup> Chao Ding,<sup>1,2,3,4</sup>  
Xiangbin Cai,<sup>1,2,3,4</sup> Haoran Zhang,<sup>1,2,3,4</sup> Xiongfeng Ma,<sup>5,\*</sup> and Weibo Gao<sup>1,2,3,4,†</sup>

<sup>1</sup>*School of Electrical and Electronic Engineering,*

*Nanyang Technological University, Singapore 639798, Singapore*

<sup>2</sup>*Division of Physics and Applied Physics, School of Physical and Mathematical Sciences,*

*Nanyang Technological University, Singapore 637371, Singapore*

<sup>3</sup>*Centre for Quantum Technologies, National University of Singapore, Singapore, Singapore*

<sup>4</sup>*Quantum Science and Engineering Centre (QSec),*

*Nanyang Technological University, Singapore, Singapore*

<sup>5</sup>*Center for Quantum Information, Institute for Interdisciplinary  
Information Sciences, Tsinghua University, Beijing 100084, China*

Quantum key distribution (QKD) enables information-theoretically secure communication against eavesdropping. However, phase instability remains a challenge across many QKD applications, particularly in schemes such as twin-field QKD and measurement-device-independent QKD. The most dominant source of phase fluctuation arises from the frequency offset between independent lasers. Here we propose a method to address this issue by employing a classical photodiode to compensate for the laser frequency difference. As an application of this method, we implement this technique in a mode-pairing QKD system, achieving an error rate approaching the theoretical limit and surpassing the linear key-rate bound over a fiber distance of 296.8 km. This approach provides a practical solution for frequency matching between independent lasers and can be extended to other fields requiring precise phase stabilization.

Quantum key distribution (QKD), a fundamental pillar of quantum technology, provides an information-theoretically secure means of communication, immune to the sophisticated eavesdropping techniques [1–12]. Since its first proof-of-concept demonstrations [13], QKD has rapidly progressed from theory to practice. Significant achievements, such as satellite-based QKD enabling secure intercontinental communication [14, 15] and terrestrial quantum communication [16–18], underscore its transformative impact.

Phase locking between two independent lasers is a critical challenge in quantum key distribution, including twin-field QKD [19] and mode-pairing QKD [20, 21]. While several techniques have been proposed to address this issue, existing solutions typically require either high-count-rate single-photon detectors [22, 23] or ultra-stable lasers stabilized via optical cavities [24] or acetylene absorption cells [24, 25]. However, the high cost and technical complexity of these approaches impose significant barriers to their practical implementation in large-scale quantum networks [10, 26]. In this work, we introduce a photodiode-based frequency-matching method to achieve laser phase stabilization, providing a cost-effective and experimentally feasible alternative. Furthermore, we demonstrate its successful integration into mode-pairing QKD, offering a scalable and robust solution for real-world quantum communication systems.

In the mode-pairing scheme, precisely estimating or compensating for the phase difference between paired modes is crucial for optimizing protocol performance. To achieve this, two distinct methods are employed. The first method involves transmitting reference pulses interspersed with QKD signal pulses. The phase difference

of these pulses is extracted from interference measurements using single-photon detectors, analyzed via maximum likelihood estimation [22] or fast Fourier transform [23]. The phase differences of the QKD pulses are then inferred by fitting or extrapolating from the pulse data. The second method stabilizes the phase of the pulses during transmission using technologies like optical cavities [27] or acetylene-stabilized lasers [25], enabling direct phase difference stabilization and eliminating the need for real-time estimation.

The first approach requires superconducting single-photon detectors with sufficiently high-count rates. Also, it reduces the duty cycle of QKD, demands additional modulation of reference light, and introduces significant computational overhead, making practical deployment challenging. Furthermore, the probabilistic detections and dead time of single-photon detectors necessitate more detection events and longer acquisition times to achieve reliable phase estimation. These limitations increase the phase error rate. By contrast, the second approach provides stable and precise phase estimation, but its reliance on costly and technically demanding infrastructure imposes significant barriers to large-scale deployment in quantum networks.

To address these issues, we propose a high-precision phase-estimation method that correlates interference measurements from a fast photodiode with those from single-photon detectors. The photodiode records the beat note of two frequency-matching classical beams. This signal directly reveals their instantaneous frequency offset and, consequently, the phase evolution relevant to the quantum signal. Thanks to its gigahertz-level bandwidth, the photodiode enables accurate real-time track-

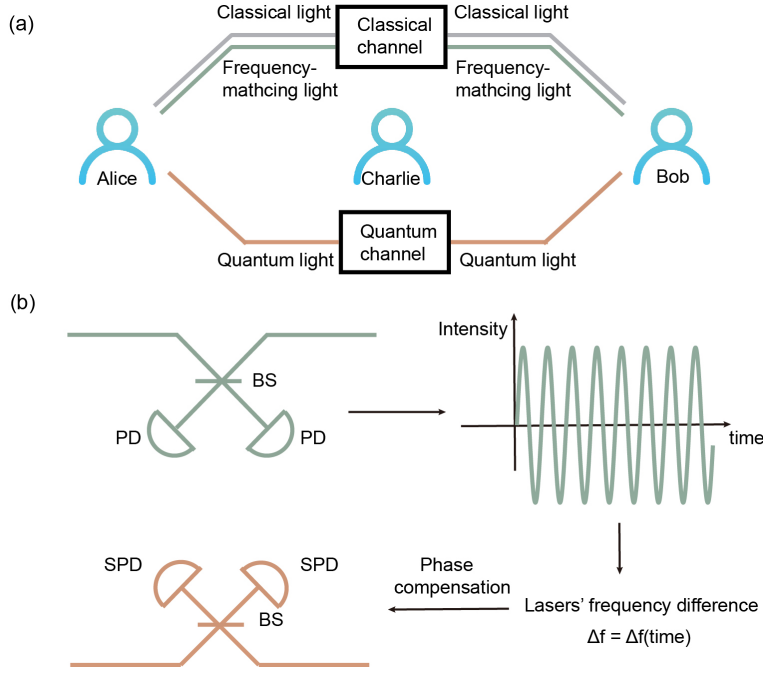


FIG. 1. (a) Alice and Bob transmit quantum light through a quantum channel to an intermediate node, Charlie, for QKD. Concurrently, they employ a classical channel to transmit classical light for conventional communication, such as synchronization of remote clocks, and utilize frequency-matching light to facilitate real-time, high-precision measurement of the frequency difference between two independent laser sources. The frequency-matching light and the classical communication light are wavelength-division multiplexed for co-fiber transmission. (b) The photodiode's measurement records the beat-note interference between the two independent lasers from Alice and Bob. The extracted frequency difference is correlated with the detection events of the single-photon detectors, enabling precise determination of the phase difference induced by the frequency offset between the independent laser sources.

ing of frequency offsets while tolerating slow drifts in the optical paths.

As shown in Fig. 1, the photodiode trace is synchronized with single-photon detection events. Since the classical frequency-matching beams co-propagate with the quantum pulses, the measured offset directly reflects the channel phase evolution. The photodiode output is a sinusoidal beat note whose phase defines the origin for reconstruction and whose frequency equals the laser offset. This enables quantum phase estimation without single-photon detectors.

Firstly, we outline the key steps of the scheme. Alice and Bob independently prepare coherent states. Alice generates a state  $|\sqrt{\mu^a}e^{i\phi^a}\rangle$ , where the intensity  $\mu^a$  is randomly chosen from  $\{0, \nu_a, \mu_a\}$  and the phase  $\phi^a$  is selected from  $\{0, \frac{2\pi}{D}, \dots, \frac{2\pi(D-1)}{D}\}$ . Bob follows the same process, preparing  $|\sqrt{\mu^b}e^{i\phi^b}\rangle$  with intensities  $\mu^b \in \{0, \nu_b, \mu_b\}$ . In this study, we set  $D = 16$ , with  $0 < \nu_a = \nu_b < \mu_a = \mu_b < 1$ . Here,  $\mu$  represents the signal state,  $\nu$  the decoy state, and  $D$  the number of phase slices in phase randomization. Alice and Bob then send their coherent states to a central measurement node (Charlie), who performs interference measurements using a balanced beam splitter and two single-photon

detectors (left and right). Successful detection events (either left or right) are postselected for pairing. Alice and Bob determine the basis and raw key values for each pair based on relative intensity, phase information, and the frequency difference acquired by the time-to-digital converter. Finally, they perform parameter estimation, information reconciliation, and privacy amplification to generate the final key. The length of the final key is given by [20]

$$K = M_{11}^Z \left[ 1 - h(e_{11}^{Z,ph}) \right] - f \sum_{\bar{\mu}} M_{\bar{\mu}} h(E_{\bar{\mu}}). \quad (1)$$

In this formulation,  $h(x)$  denotes the binary entropy function,  $f$  represents the error correction efficiency,  $M_{11}^Z$  is the single-photon  $Z$ -pair count, and  $e_{11}^{Z,ph}$  signifies the phase error rate. The key rate  $R = K/N_{\text{pair}}$ , where  $N_{\text{pair}}$  represents half the total number of rounds. A more detailed description of these steps can be found in the Supplemental Materials.

In our experimental setup, depicted in Fig 2, we employ a commercial narrow-linewidth laser operating at 1550 nm with an approximate linewidth of 1 kHz. The laser output is divided into two beams: one designated for

frequency-matching and the other for quantum light interference. The quantum light beam first passes through an intensity modulator, converting the continuous wave into pulsed light at a repetition rate of 500 MHz and a pulse width of 375 ps. Subsequently, this pulsed light enters a Sagnac loop configuration—comprising a circulator, beam splitter, phase modulator, and optical fibers—which further modulates the light intensity to produce the desired decoy states [28]. The light exiting the Sagnac loop is then phase-randomized by a phase modulator before being transmitted from the sender’s end.

After traversing the long optical fiber spool, the two quantum light beams reach Charlie, where polarization alignment is achieved using two polarization feedback modules. Each module comprises an electric polarization controller, a polarization beam splitter, and a single-photon detector. By adjusting the voltage of the electric polarization controller based on the photon counts from the the single-photon detectors, one single-photon detector’s count is minimized, enhancing the interference contrast between Alice and Bob. The detectors monitoring the two paths post-interference at the beam splitter have a detection efficiency of 63% and a dark count rate of 30 Hz. The optical loss at Charlie corresponds to an attenuation of 1.91 dB.

In the frequency-matching light interference process, the optical signals from Alice and Bob undergo the optical attenuation, serving as an alternative to optical fibers. This substitution is justified by the fact that the fiber in the frequency compensation channel has a negligible impact on frequency measurement. The rationale for using attenuation as a substitute for optical fiber is provided in the Supplementary Material. This method enables rapid frequency difference measurements, typically achieving results within tens of nanoseconds. At Charlie’s side, the output light from the BS is detected by the photodiodes (Thorlabs PDB480C), converted into an electrical signal, and subsequently processed using a time-to-digital converter for high-precision timing processing.

We present the optimized intensity parameters for distances of 197.91 km and 296.80 km in Table 2. For the X-basis, we measured the temporal delay between the signals from the single-photon detector and the photodiode for two fiber lengths, correlated the classical and quantum light interference results, and calculated the error rate. For the Z-basis, we achieved a high signal-to-noise extinction ratio using the intensity modulator and Sagnac ring, as evidenced by the observed error rate. A detailed description of the experimental procedure is provided in the Supplementary Material.

Under the 197.91 km fiber condition, we achieved a secure key rate of  $6.11 \times 10^{-6}$ , with a maximum pairing time of 10  $\mu$ s. The X-basis bit error rate was 26.92% for the pairing time of 10  $\mu$ s, slightly exceeding the theoretical minimum of 25% required for key generation. For the

TABLE I. The optimized intensity parameters.  $\eta$  represents the detector efficiency,  $\mu$  and  $\nu$  denote the average photon numbers of the signal and decoy states, respectively.  $p_\mu$  and  $p_\nu$  are the corresponding sending probabilities, and  $f$  is the error correction factor, which is 1.06 [29].

Parameter	197.91 km	296.80 km
Channel Loss (dB)	38.83	57.36
Sent Pulses	$2.08 \times 10^{12}$	$9.86 \times 10^{12}$
$\mu$	0.3958	0.3591
$\nu$	0.0275	0.0232
$p_\mu$	0.15	0.25
$p_\nu$	0.25	0.30
$f$	1.06	1.06

296.80 km fiber, we extended the maximum pairing time to 20  $\mu$ s, yielding a key generation rate of  $2.45 \times 10^{-7}$ , which surpasses the PLOB bound of  $1.20 \times 10^{-7}$ . At this distance, the X-basis error rate was 27.76% for the pairing time of 20  $\mu$ s.

Fig. 3 illustrates the temporal fluctuations in error rates for both the X- and Z-basis across two different fiber lengths. For the X-basis, the theoretical minimum error rate is 25%. The observed system error arises from modulation-induced errors and phase uncertainties introduced by the fiber, which become more pronounced as the fiber length increases. A primary advantage of our frequency-matching method is that the measured phase error between the two matched pulses is predominantly determined by the phase difference arising from frequency mismatch, which occurs on a timescale of tens of nanoseconds. Additional details are provided in the Supplementary Material.

Ideally, the theoretical error rate for the Z-basis can be reduced to zero. However, in practical implementations, errors primarily originate from incomplete extinction, dark counts, and ambient light noise. In our setup, the error rate in the Z-basis is consistently maintained below 0.3%.

Additionally, we examine how the X-basis error rate varies with the maximum pairing length, as depicted in Fig. 4. In the limit of a vanishing pairing length, optical pulse modulation imperfections dominate the error contribution, consistent with previous studies [25, 27]. As the pairing length increases, the error rate correspondingly rises, primarily due to phase fluctuations induced by fiber perturbations over the pairing duration.

We further examine the variation in the number of paired events under the mode-pairing QKD protocol at a transmission distance of 296.80 km, as represented by the orange line in the figure. Notably, when the maximum pairing length extends to 50  $\mu$ s, the number of pairings begins to saturate. Considering both the pairing rate and

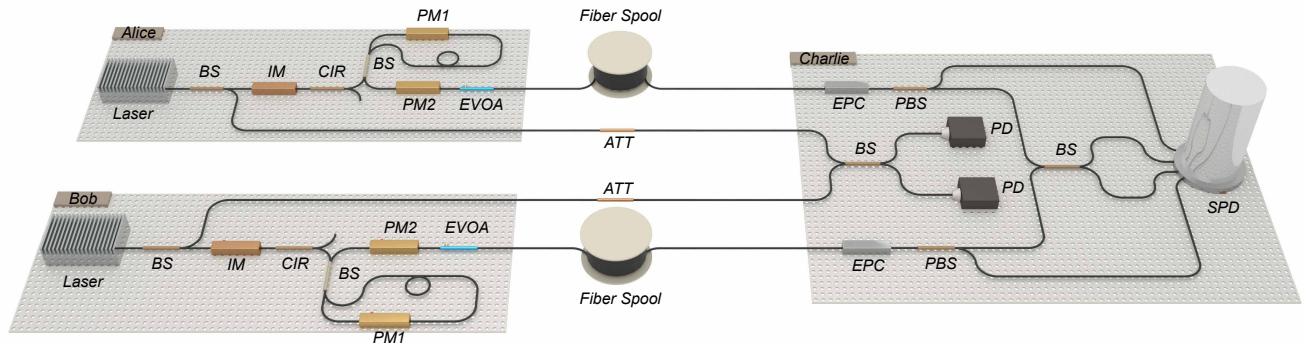


FIG. 2. Experimental Setup. Alice and Bob employ narrow-linewidth lasers as light sources, splitting the output into two beams. One beam is directed to Charlie for interference, where photodiodes facilitate frequency matching. The second beam undergoes quantum light modulation, including chopping and decoy state modulation via an intensity modulator and a Sagnac loop, comprising a circulator, beam splitter, phase modulator, and optical fibers. A phase modulator applies 16 distinct phase levels for phase randomization. The modulated quantum light pulses are transmitted to Charlie, where polarization feedback aligns the polarization of the two beams. Interference is then performed using a beam splitter. The resulting signals from both PDs and single-photon detectors are processed through a time-to-digital converter for post-processing, ultimately generating secure keys. BS: beam splitter; IM: intensity modulator; CIR: fiber optical circulator; PM: phase modulator; EVOA: electrical variable optical attenuator; EPC: electric polarization controller; PBS: polarizing beam splitter; PD: photodiode; SPD: single-photon detector.

TABLE II. Comparison of phase estimation methods. The table reports the X-basis error rate ( $E_x$ ) values from different experiments conducted under fiber conditions of approximately 200 km. For mode-pairing QKD protocols, the theoretical minimum value of  $E_x$  is 25%.

Experiment	Method	SNSPD for phase compensation	Optical frequency reference	X-basis error
Zhou <i>et al.</i> [27]	High-finesse cavities	Not required	Required	26.94%
Zhang <i>et al.</i> [30]	Data post-processing	Required	Not required	27.77%
Shao <i>et al.</i> [31]	Data post-processing	Required	Not required	28.91%
This work	Simple photodiode	Not required	Not required	26.92%

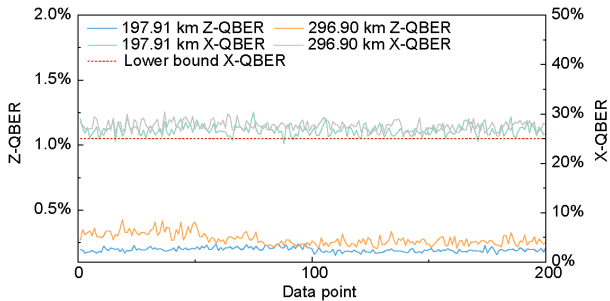


FIG. 3. Error drift. Data point represents the sequence number of data, with each data point collected approximately every 30 seconds, as the size of every data file is fixed.

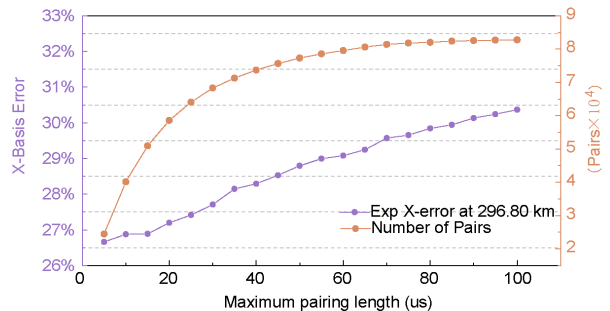


FIG. 4. X-basis error varied with maximum pairing length at 296.80 km. Here the handling data is  $3.25 \times 10^{11}$ .

error performance, we select a maximum pairing length of 20  $\mu$ s. For practical applications, the optimal maximum pairing length can be determined based on photon transmittance, as discussed in Ref. [22].

We compare our results with previous mode-pairing QKD experiments, as summarized in Table II. Aside from this work, mode-pairing QKD implementations that exceed the rate-transmittance linear bound predominantly utilize optical cavities, commercial acetylene-stabilized

laser systems, or data post-processing based on high-count-rate single-photon detectors. Our method offers a more practical and experimentally accessible implementation. Moreover, it achieves an X-basis error rate approaching the fundamental limit.

In summary, our approach eliminates the need for high-finesse optical cavities, commercial acetylene-stabilized lasers, and high-count-rate single-photon detector-based data post-processing, while enabling seamless integra-

tion with classical communication channels. Moreover, incorporating an erbium-doped fiber amplifier into the frequency-matching optical path can extend communication distances by compensating for transmission losses [32], enhancing its feasibility for field deployment. Additionally, employing multi-wavelength multiplexing in conjunction with this technique for mode-pairing QKD can further improve the key generation rate. By significantly reducing system complexity and cost, this method provides a practical and efficient framework for mode-pairing QKD, demonstrating strong potential for large-scale deployment in quantum networks. Furthermore, it offers a promising approach for integration into satellite-ground links, expanding its applicability in quantum communications.

This work is supported by the National Research Foundation, Singapore and A\*STAR under its Quantum Engineering Programme (NRF2021-QEP2-01-P02, National Quantum-Safe Network, NRF2021-QEP2-04-P01, NRF2022-QEP2-02-P13), A\*STAR (M21K2c0116, M24M8b0004), Singapore National Research foundation (NRF-CRP22-2019-0004, NRF2023-ITC004-001, NRFCRP30-2023-0003, NRF-MSG-2023-0002), Singapore Ministry of Education Tier 2 Grant (MOE-T2EP50222-0018), National Natural Science Foundation of China Grant No. 12174216. We thank the support from Dieter Schwarz Stiftung gGmbH.

---

\* [xma@tsinghua.edu.cn](mailto:xma@tsinghua.edu.cn)

† [wbgao@ntu.edu.sg](mailto:wbgao@ntu.edu.sg)

- [1] C. H. Bennett and G. Brassard, Quantum Cryptography: Public Key Distribution and Coin Tossing, in *Proceedings of the IEEE International Conference on Computers, Systems and Signal Processing* (IEEE Press, New York, 1984) pp. 175–179.
- [2] A. K. Ekert, Quantum cryptography based on bell’s theorem, *Physical review letters* **67**, 661 (1991).
- [3] H.-K. Lo and H. F. Chau, Unconditional security of quantum key distribution over arbitrarily long distances, *science* **283**, 2050 (1999).
- [4] P. W. Shor and J. Preskill, Simple proof of security of the bb84 quantum key distribution protocol, *Physical review letters* **85**, 441 (2000).
- [5] D. Gottesman, H.-K. Lo, N. Lütkenhaus, and J. Preskill, Security of quantum key distribution with imperfect devices, *Quantum Info. Comput.* **4**, 325–360 (2004).
- [6] V. Scarani, H. Bechmann-Pasquinucci, N. J. Cerf, M. Dušek, N. Lütkenhaus, and M. Peev, The security of practical quantum key distribution, *Reviews of modern physics* **81**, 1301 (2009).
- [7] G. Brassard, N. Lütkenhaus, T. Mor, and B. C. Sanders, Limitations on practical quantum cryptography, *Physical review letters* **85**, 1330 (2000).
- [8] C. H. Bennett, G. Brassard, and N. D. Mermin, Quantum cryptography without bell’s theorem, *Physical review letters* **68**, 557 (1992).
- [9] R. Renner, N. Gisin, and B. Kraus, Information-theoretic security proof for quantum-key-distribution protocols, *Physical Review A—Atomic, Molecular, and Optical Physics* **72**, 012332 (2005).
- [10] D. Ribezzo, M. Zahidy, I. Vagniluca, N. Biagi, S. Francesconi, T. Occhipinti, L. K. Oxenløwe, M. Lončarić, I. Cvitić, M. Stipčević, *et al.*, Deploying an inter-european quantum network, *Advanced Quantum Technologies* **6**, 2200061 (2023).
- [11] R. Renner, Security of quantum key distribution, *International Journal of Quantum Information* **6**, 1 (2008).
- [12] I. Devetak and A. Winter, Distillation of secret key and entanglement from quantum states, *Proceedings of the Royal Society A: Mathematical, Physical and engineering sciences* **461**, 207 (2005).
- [13] C. H. Bennett, F. Bessette, G. Brassard, L. Salvail, and J. Smolin, Experimental quantum cryptography, *Journal of cryptology* **5**, 3 (1992).
- [14] S.-K. Liao, W.-Q. Cai, J. Handsteiner, B. Liu, J. Yin, L. Zhang, D. Rauch, M. Fink, J.-G. Ren, W.-Y. Liu, Y. Li, Q. Shen, Y. Cao, F.-Z. Li, J.-F. Wang, Y.-M. Huang, L. Deng, T. Xi, L. Ma, T. Hu, L. Li, N.-L. Liu, F. Koidl, P. Wang, Y.-A. Chen, X.-B. Wang, M. Steindorfer, G. Kirchner, C.-Y. Lu, R. Shu, R. Ursin, T. Scheidl, C.-Z. Peng, J.-Y. Wang, A. Zeilinger, and J.-W. Pan, Satellite-relayed intercontinental quantum network, *Phys. Rev. Lett.* **120**, 030501 (2018).
- [15] R. Bedington, J. M. Arrazola, and A. Ling, Progress in satellite quantum key distribution, *npj Quantum Information* **3**, 30 (2017).
- [16] Y.-A. Chen, Q. Zhang, T.-Y. Chen, W.-Q. Cai, S.-K. Liao, J. Zhang, K. Chen, J. Yin, J.-G. Ren, Z. Chen, *et al.*, An integrated space-to-ground quantum communication network over 4,600 kilometres, *Nature* **589**, 214 (2021).
- [17] V. Martin, J. P. Brito, L. Ortíz, R. Mendez, J. Buruaga, R. Vicente, A. Sebastian-Lombrana, D. Rincon, F. Perez, C. Sanchez, *et al.*, Madqci: a heterogeneous and scalable sdn-qkd network deployed in production facilities, *npj Quantum Information* **10**, 80 (2024).
- [18] Y. Liu, W.-J. Zhang, C. Jiang, J.-P. Chen, C. Zhang, W.-X. Pan, D. Ma, H. Dong, J.-M. Xiong, C.-J. Zhang, *et al.*, Experimental twin-field quantum key distribution over 1000 km fiber distance, *Physical Review Letters* **130**, 210801 (2023).
- [19] M. Lucamarini, Z. L. Yuan, J. F. Dynes, and A. J. Shields, Overcoming the rate–distance limit of quantum key distribution without quantum repeaters, *Nature* **557**, 400 (2018).
- [20] P. Zeng, H. Zhou, W. Wu, and X. Ma, Mode-pairing quantum key distribution, *Nature Communications* **13**, 3903 (2022).
- [21] Y.-M. Xie, Y.-S. Lu, C.-X. Weng, X.-Y. Cao, Z.-Y. Jia, Y. Bao, Y. Wang, Y. Fu, H.-L. Yin, and Z.-B. Chen, Breaking the rate-loss bound of quantum key distribution with asynchronous two-photon interference, *PRX Quantum* **3**, 020315 (2022).
- [22] H.-T. Zhu, Y. Huang, H. Liu, P. Zeng, M. Zou, Y. Dai, S. Tang, H. Li, L. You, Z. Wang, *et al.*, Experimental mode-pairing measurement-device-independent quantum key distribution without global phase locking, *Physical Review Letters* **130**, 030801 (2023).
- [23] W. Li, L. Zhang, Y. Lu, Z.-P. Li, C. Jiang, Y. Liu, J. Huang, H. Li, Z. Wang, X.-B. Wang, *et al.*, Twin-field quantum key distribution without phase locking, *Physi-*

- cal Review Letters **130**, 250802 (2023).
- [24] J.-P. Chen, F. Zhou, C. Zhang, C. Jiang, F.-X. Chen, J. Huang, H. Li, L.-X. You, X.-B. Wang, Y. Liu, *et al.*, Twin-field quantum key distribution with local frequency reference, Physical Review Letters **132**, 260802 (2024).
- [25] C. Ge, L. Zhou, J. Lin, H.-L. Yin, Q. Zeng, and Z. Yuan, Post-measurement pairing quantum key distribution with local optical frequency standard, Quantum Science and Technology (2024).
- [26] M. Sasaki, M. Fujiwara, H. Ishizuka, W. Klaus, K. Wakui, M. Takeoka, S. Miki, T. Yamashita, Z. Wang, A. Tanaka, *et al.*, Field test of quantum key distribution in the tokyo qkd network, Optics express **19**, 10387 (2011).
- [27] L. Zhou, J. Lin, Y.-M. Xie, Y.-S. Lu, Y. Jing, H.-L. Yin, and Z. Yuan, Experimental quantum communication overcomes the rate-loss limit without global phase tracking, Physical Review Letters **130**, 250801 (2023).
- [28] E. J. Post, Sagnac effect, Reviews of Modern Physics **39**, 475 (1967).
- [29] B.-Y. Tang, C.-Q. Wu, W. Peng, B. Liu, and W.-R. Yu, Polar-code-based information reconciliation scheme with the frozen-bit erasure strategy for quantum key distribution, Physical Review A **107**, 012612 (2023).
- [30] L. Zhang, W. Li, J. Pan, Y. Lu, W. Li, Z.-P. Li, Y. Huang, X. Ma, F. Xu, and J.-W. Pan, Experimental mode-pairing quantum key distribution surpassing the repeaterless bound, Physical Review X **15**, 021037 (2025).
- [31] S.-F. Shao, L. Zhou, J. Lin, M. Minder, C. Ge, Y.-M. Xie, A. Shen, Z. Yan, H.-L. Yin, and Z. Yuan, High-rate measurement-device-independent quantum communication without optical reference light, Physical Review X **15**, 021066 (2025).
- [32] H. Liu, C. Jiang, H.-T. Zhu, M. Zou, Z.-W. Yu, X.-L. Hu, H. Xu, S. Ma, Z. Han, J.-P. Chen, *et al.*, Field test of twin-field quantum key distribution through sending-or-not-sending over 428 km, Physical review letters **126**, 250502 (2021).